J. Geotech. Eng., JSCE, No. 778/III-69, 1-15, 2004 December

A POSTERIORI ERROR ESTIMATE AND *H*-ADAPTIVE FE ANALYSIS OF LIQUEFACTION WITH LARGE DEFORMATION

Xiaowei TANG[1] and Tadanobu SATO[2]

[1]Member of JSCE, Docroral Graduate student, Graduate School of Engineering, Kyoto University
(Gokasho, Uji, Kyoto 611-0011, Japan)
E-mail:tang@catfish.dpri.kyoto-u.ac.jp
[2]Member of JSCE, Professor, Disaster Prevention Research Institute, Kyoto University
(Gokasho, Uji, Kyoto 611-0011, Japan)
E-mail:sato@catfish.dpri.kyoto-u.ac.jp

FEM error due to discretization in the space domain causes inaccuracies in the nonlinear dynamic analysis of saturated soil, especially in the analysis of liquefaction considering large deformation. An adaptive strategy includes an error estimate and mesh refinement, in which the approximation is refined successively to a predetermined standard of accuracy, is essential to the effective use of finite element codes for practical analyses. In this paper, a posteriori error estimate procedure and *h*-adaptive FE are applied to liquefaction analysis of saturated soil using the elasto-plastic constitutive model and updated Lagrangian formulation. The advantage of this method is shown by the analysis of three numerical examples of saturated soil.

Key Words : *error estimate, adaptivity, liquefaction, large deformation, dynamic analysis*

1. INTRODUCTION

Nonlinear FEM analysis of liquefaction is being used in many of areas of research and for practical engineering problems because liquefaction causes serious damage to many types of constructions during earthquakes. New effective constitutive models for liquefiable soil have been developed to simulate the material nonlinear behavior of soil. Owing to the large deformation caused by liquefaction, the finite deformation theory is more suitable than the normal theory based on the assumption of small deformation, and it has been used in FEM analysis of liquefaction. Although it effectively deals with the geometrical non-linearity of liquefied soil, some problems should be noted. As a type of numerical approximation method, errors are inevitable in analysis results obtained by the finite element method. The finite element method solution does not always guarantee the desired accuracy, sometimes causing serious analysis problems. For example, in liquefaction analysis of saturated soil considering large deformation, when a coarse mesh is used to save time, error causes severe distortion of the elements and sometimes calculation stops unexpectedly. The accuracy of FEM remains a major concern, particularly when a non-linear material response occurs, or large deformation is involved.

FEM error is caused by discretization. Evidently, reducing the size of the elements uniformly during discretization minimizes error, but the number of nodes and elements are increased as is the calculation time. Our objective was to use a fine mesh in the area of large error and a normal or coarse mesh in the low error one.A method called the adaptive technique or adaptive mesh refinement has been developed and used to solve this error problem. It has been used successfully in many fields including solid and fluid mechanics, for linear and nonlinear problems, in order to solve static and transient behavior of 2 and 3

dimensional continua. Our aim was to use adaptive mesh refinement for the liquefaction analysis of soil considering large deformation.

An adaptive FE method, in which approximation is refined successively to reach a predetermined standard of accuracy, is essential for the effective use of finite element codes in practical analyses. The procedure, which refines the mesh of the finite elements according to an error indicator, has two parts: error estimate and mesh refinement. A main feature of this method is that it involves local, rather than global, refinement. In the error estimation, error is defined as the difference between the approximate and exact solutions of certain variables, such as displacement, stress, and strain. Generally, it is estimated by means of the energy norm or L_2 norm. Mesh refinement includes *h*-, *p*-, *hp*-, and *r*-refinement. *H*-refinement is the simple reduction of subdivision size, including remeshing and fission.

The *h*-adaptive FE method is here applied to liquefaction analysis of saturated soil considering large deformation. An effective cyclic elasto-plastic model[1)-3)] based on Biot's two-phase mixture theory and the kinematic hardening rule was adopted to simulate the non-linear behavior of saturated soil. The u-p formulation was used for the governing equations that describe the coupled problem in terms of soil skeleton displacement and excess pore water pressure. The updated Lagrangian method was used in the formulation to account for large deformation. The dynamic equations were solved by the Newmark-β method. Bilinear, four-node quadrilateral elements were used in the discretization. To estimate liquefied soil error, an error criterion based on the L_2-projection of stress or strain was selected. Because it is impossible to obtain the exact value, we evaluated the more accurate variables by a recovery procedure[8)-17)] in which least square technique is used in order to make a comparision with the approximate solution. The calculation is very simple and easy to use in programming, and the result is reliable. A fission procedure[18)-20)] belonging to *h*-refinement was adopted for mesh refinement. After the calculation of one step, elements which exceed a given error limit are fissioned into 4 elements and the next step processed. The flow chart of this procedure is shown in **Fig.1**.

A program based on this method was coded in Fortran. Three numerical examples are given: the compression of saturated sand by stepwise loading, liquefied sand flow problems, and the seismic response of an embankment resting on liquefiable sand. The efficiency of this technique for liquefiable soil analysis is shown.

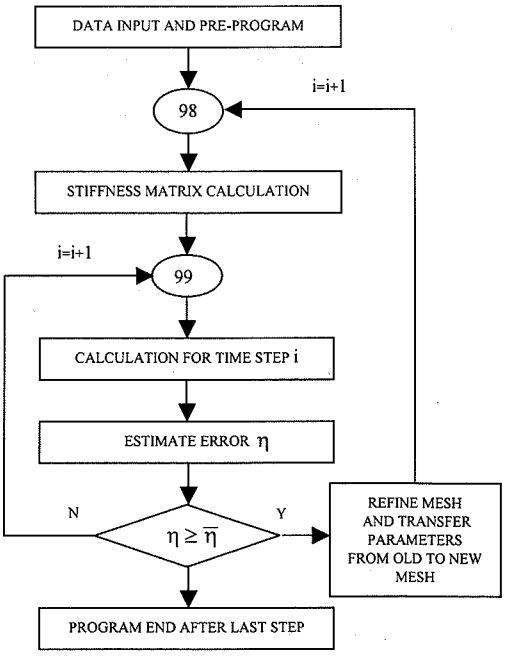

Fig.1 A posteriori error estimate and h-adaptivity ($\bar{\eta}$ is the desired limit of relative error)

2. BASIC FINITE ELEMENT METHOD AND UPDATED LAGRANGIAN FORM

The two-phase mixture theory is used in the analysis of liquefaction. It was proposed by Biot[4)] in 1962 and has been widely used for the non-linear analysis of saturated soils. A u-p formulation in the mixed FEM based on the assumption of small deformation developed by Akai and Tamura[5)] in 1982. We use a new version of this scheme as modified by Di and Sato[6)-7)], in which the updated Lagrangian formulation is adopted. The derivation of the governing equations is introduced here.

(1) Constitutive equation

An effective cyclic elasto-plastic constitutive model was used to simulate the non-linear behavior of saturated soil. It is developed by Oka[1)-3)] based on Biot's two-phase mixture theory and the kinematic hardening rule. The stress-dilatancy relationship and cumulative strain-dependent characteristics of the plastic shear modulus have been taken into account. The simulation results for saturated soil agree with the experimental results, even for the liquefaction process. This constitutive model is incorporated in a mixed

FE-FD coupled method.

The general linear relationship between the objective stress and deformation rates is

$$\dot{\sigma}^{J}_{ij} = D_{ijkl} l_{kl} - \dot{p}\delta_{ij} \quad (1)$$

where $\dot{p}$ is the of pore water pressure rate, l_{kl} the symmetric deformation rate tensor, δ_{ij} the Kronecker delta, and D_{ijkl} the instantaneous stiffness of the material. The Jaumann stress rate, which gives an objective measure of the stress rate, was used in the present formulation.

$$\dot{\sigma}^{J}_{ij} = \dot{\sigma}_{ij} - \sigma_{ik}\omega_{jk} - \sigma_{jk}\omega_{ik} \quad (2)$$

where $\dot{\sigma}_{ij}$ is the Cauchy stress tensor rate and ω_{ij} the skew symmetric spin tensor defined by

$$\omega_{ij} = \tfrac{1}{2}(v_{i,j} - v_{j,i}) \quad (3)$$

where v_i is the velocity.

(2) Equilibrium equation

According to Biot's two-phase mixture theory, the equation of motion for total saturated soil is

$$\sigma_{ij,j} + \rho b_i - \rho\ddot{u}_i - \rho_f\left(\ddot{w}_i + \dot{w}_k \dot{w}_{i,k}\right) = 0 \quad (4)$$

where σ_{ij} is the Cauchy total stress, $\dot{w}_{ij}$ and $\ddot{w}_{ij}$ are the pseudo velocity and acceleration of the pore fluid relative to the soil skeleton.

Neglecting acceleration of the pore fluid, the equilibrium equation for saturated soil is

$$\sigma_{ij,j} + \rho b_i - \rho\ddot{u}_i = 0 \quad (5)$$

Integrating in the spatial domain, we obtain the weak form of the equilibrium equation at time t+dt:

$$\int_{+dt V} {}^{t+dt}\rho\, {}^{t+dt}\ddot{u}_i \delta v_i \, d^{t+dt}V + \int_{+dt V} \left(\int_{t_1}^{t_2} \dot{S}_{ij} dt\right)\delta\dot{E}_{ij}\, d^{t+dt}V = \int_{+dt A} {}^{t+dt}T_i \delta v_i \, d^{t+dt}A + \int_{+dt V} {}^{t+dt}\rho\, {}^{t+dt}b_i \delta v_i \, d^{t+dt}V - \int_{+dt V} {}^{t+dt}\sigma_{ij}\delta\dot{E}_{ij}\, d^{t+dt}V \quad (6)$$

where v_i is the velocity of the solid skeleton. b_i body force on the volume, V, of the porous medium, T_i the traction on the surface A, E_{ij} the Lagrangian strain tensor, and S_{ij} the second Piola-Kirchhoff stress tensor.

(3) Constitutive equation

From Biot's two-phase mixture theory, neglecting the acceleration of fluid phase, the pore fluid equilibrium equation is

$$(np)_{,i} - n\rho_f b_i + n\gamma_f k^{-1}\dot{w}_i + n\rho_f \ddot{u}_i = 0 \quad (7)$$

where n is the porosity, ρ_f the density of the pore fluid, γ_f the weight in unit volume, and k the permeability coefficient.

The mass conservation equation for fluid flow is simplified as Eq.(7) by assuming that the porosity distribution of the medium is sufficiently smooth, solid partials are incompressible, the initial strain rate is 0, and by neglecting thermal expansion of the fluid.

$$\dot{w}_{i,i} + \dot{\varepsilon}_{ii} + \frac{n}{K_f}\dot{p} = 0 \quad (8)$$

where K_f is Young's modular of the pore fluid.

Combining Eqs.(6) and (7) gives a simple form of continuity equation;

$$\rho_f \ddot{\varepsilon}_{ii} - \frac{\partial^2 p}{\partial x_i^2} - \frac{\gamma_f}{k}\left(\dot{\varepsilon}_{ii} - \frac{n}{K_f}\dot{p}\right) = 0 \quad (9)$$

Integrating over the porous medium volume, the weak form of Eq.(8) is

$$-\int_{+dt V} {}^{t+dt}\rho_f\, {}^{t+dt}\ddot{\varepsilon}_{ii}\, d^{t+dt}V - \int_{+dt V} {}^{t+dt}p_{,ii}\, d^{t+dt}V - \int_{+dt V} \frac{\gamma_f}{k}\, {}^{t+dt}\dot{\varepsilon}_{ii}\, d^{t+dt}V + \int_{+dt V} \frac{n\gamma_f}{kK_f}\, {}^{t+dt}\dot{p}\, d^{t+dt}V = 0 \quad (10)$$

(4) Updated Lagrangian FEM equations

We used the updated Lagrangian description belonging to the Lagrangian family in order to deal with the large deformation of saturated soil. In this formulation, all variables at time t are taken as the reference configuration of the variables at time t+Δt. The reference configuration is updated at each calculation step.

Referring all stresses, strains and deformations at time t+Δt to the current configuration at time t by use of the updated Lagrangian method[1], the weak form of the equilibrium and continuity equation at time t+dt are rewritten as Eq. (11) and Eq. (12);

$$\int_{tV} {}^{t}\rho\, {}^{t}\ddot{u}_i \delta v_i \, d^{t}V + \int_{tV} \left(\int_{t_1}^{t_2} \dot{S}_{ij} dt\right)\delta\dot{E}_{ij}\, d^{t}V = \int_{tA} {}^{t+dt}T_i \delta v_i \, d^{t}A + \int_{tV} {}^{t}\rho\, {}^{t+dt}b_i \delta v_i \, d^{t}V - \int_{tV} {}^{t}\sigma_{ij}\delta\dot{E}_{ij}\, d^{t}V \quad (11)$$

$$-\int_{tV} {}^{t}\rho_f\, {}^{t+dt}\ddot{\varepsilon}_{ii}\, d^{t}V - \int_{tV} {}^{t+dt}p_{,ii}\, d^{t}V - \int_{tV} \frac{\gamma_f}{k}\, {}^{t+dt}\dot{\varepsilon}_{ii}\, d^{t}V + \int_{tV} \frac{n\gamma_f}{kK_f}\, {}^{t+dt}\dot{p}\, d^{t}V = 0 \quad (12)$$

where, b_i body force on the volume, V, of the porous medium, T_i traction on the surface A, E_{ij} the Lagrangian strain tensor, and S_{ij} the second Piola-Kirchhoff stress tensor.

Discretizing Eq.(11) in the space domain by the finite element method, gives the final form of the equilibrium equation;

$$[M]\{{}^{t+dt}\ddot{U}\} + [K_L]\{dU\} + [K_{NL}]\{dU\} + [K_V]\{{}^{t+dt}p_E\} = \{F_A\} + \{F_V\} - \{F'\} \quad (13)$$

where [M] is the mass matrix of the porous medium, $[K_L]$ the stiffness matrix of the elements, $[K_{NL}]$ the geometric stiffness matrix, $\{p_E\}$ the excess pore pressure vector at the element center, and $[K_V]$ a matrix coupling the displacement increment with

excess pore water pressure. $\{F_A\}$, $\{F_V\}$, and $\{F'\}$ respectively are the load vector expressing the effect of the element surface traction force, the element body force, and the element initial force.

In the same way, we obtain the final form of the equilibrium equation as Eq. (14);

$$-\rho_f[K_V]\{\ddot{U}\}-\frac{\gamma_w}{k}[K_V]\{\dot{U}\}+[\alpha]\{^{t+dt}p_E\}+$$
$$\int_{t_V}\frac{n\gamma_w}{kK_f}[N_p]d^tV\{^{t+dt}\dot{p}_E\}=0 \qquad (14)$$

where p is approximated by $[N_P]\{p_E\}$, p_E the excess pore pressure at the center of each element, and $[\alpha]\{^{t+dt}p_E\}$ the difference expression of the second term in Eq. (12).

Adding Rayleigh damping to Eqs.(13) and (14), gives the final finite element formulas as the u-p form for dynamic analysis of the porous medium. The Newmark-β method for time domain integration is used to solve the dynamic equations.

3. POSTERIORI ERROR ESTIMATE

Error estimate is the first and most important procedure of adaptivity giving an indication of the next step, mesh refinement. The error for each element, which is due to spatial discretization in the FEM, is calculated in this step. The elements which need to be refined then can be distinguished from those which do not by comparing the errors with an acceptable limit. FEM accuracy therefore is improved in addition to saving degrees of freedom. There are two distinct types of general error estimates, recovery-based and residual-based one. A posteriori error estimate procedure that depends on local smoothing of variables based on a least squares fit scheme was used. It is a recovery-based estimate type.

(1) Definition and Measure of Error

Error is defined as the difference between the exact solution and value of the finite element approximation. Variables considered in the error estimate are displacement, strain, and stress. For example, an error in strain is described as

$$e_\sigma=\varepsilon^*-\varepsilon^h \qquad (15)$$

and an error in stress as

$$e_\sigma=\sigma^*-\sigma^h \qquad (16)$$

where ε^* and σ^* are the exact solutions, ε^h and σ^h the values of the finite element approximation.

To explain the approximate value of FEM and the exact solution, a one-dimensional linear approximation of strain ε^h and ε^* is shown in **Fig.2**.

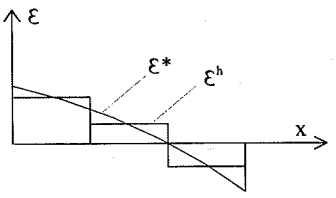

Fig.2 Approximate values and exact solution

The direct definitions of error described in Eqs.(15) and (16) are not convenient for use in the process of error estimation. Usually, scalar norms, such as energy or L_2 norms, are used to measure error. This scalar measure corresponds to the square root of the quadratic error. In this study, we used the L_2 norm to measure error, as it can be associated with errors of any quantity. For the strain or stress in the element *i*, the L_2 norm of the error, e_i, is

$$\|e_i\|=\left(\int_{V_i}\{e\}^T\{e\}dv/V_i\right)^{1/2} \qquad (17)$$

In the practical adaptivity process, a relative percentage error generally is used because it is more easily interpreted. Its definition for the *i*th element is

$$\eta_i=\frac{\|e_i\|}{\|e_i\|+\|\varepsilon_i^h\|}\times 100\% \qquad (18)$$

It is clear that the energy and L_2 norms are related to the strain energy. This relationship is shown as follows:

Considering the physical relationship between the stress and strain,

$$\{\varepsilon\}=[D]^{-1}\{\sigma\} \qquad (19)$$

the total potential energy, A, of a system predicted by the approximate solution of FEM is

$$A=\int_V\tfrac{1}{2}\{\sigma^h\}^T[D]^{-1}\{\sigma^h\}dv-\{R\}^T\{\bar{u}\} \qquad (20)$$

where $\{R\}$ is the vector of the loads and the reaction acting on the nodes, $\{\bar{u}\}$ the vector of displacement on the nodes, and [D] the stiffness matrix.

Assuming infinitesimal displacement $\{d\bar{u}\}$ on nodes, from the principle of virtual work,

$$\{R\}^T\{d\bar{u}\}=\int_V\{d\varepsilon^h\}^T\{\sigma^*\}dv \qquad (21)$$

Substituting Eq. (21) in Eq. (20), the total potential energy is

$$A=\int_V\tfrac{1}{2}\{\sigma^h\}^T[D]^{-1}\{\sigma^h\}dv-\int_V\{\sigma^*\}^T\{\varepsilon^h\}dv$$
$$=\int_V\tfrac{1}{2}\{\sigma^h\}^T[D]^{-1}\{\sigma^h\}dv-\int_V\{\sigma^*\}^T[D]^{-1}\{\sigma^h\}dv \qquad (22)$$

Eq. (22) can be put into another form;

$$A=\int_V\tfrac{1}{2}\{\sigma^h-\sigma^*\}^T[D]^{-1}\{\sigma^h-\sigma^*\}dv+c \qquad (23)$$

where c is the constant without relation to nodal

displacement.

Using another physical relationship between the stress and strain,

$$\{\sigma\} = [D]\{\varepsilon\} \tag{24}$$

By the same derivation method, the same conclusion for error of strain is

$$A = \int_V \tfrac{1}{2}\{\varepsilon^h - \varepsilon^*\}^T [D]\{\varepsilon^h - \varepsilon^*\} dv + c \tag{25}$$

From Eqs. (23) and (25), the total potential energy is interpreted as a weighted, stress error squared quantity. When the size of an element is small enough, the unweighted, error squared quantity corresponds to the weighted error squared quantity. The relationship between the L_2 norm of error and the total potential energy is ensured. Because the L_2 norm of error is a positive definite function, the global L_2 norm of error is the sum of the local L_2 norms of error. Then the L_2 norm can be used to measure error, not only in the global mesh, but in a local element.

(2) Local smoothing by extrapolation

In the error estimate process, the more accurate values rather than the exact solution are used to calculate errors because the exact solution is not easy or impossible to obtain. In the past twenty years, recovery procedures have been developed and used widely. We use a local smoothing procedure, a kind of recovery for such interest variables as stress and strain. It is based on the least squares technique.

The conventional least squares smoothing method gives a smoothing function for a two- dimensional problem;

$$P(x,y) = a_0 + a_1 x + a_2 y + a_3 xy + a_4 x^2 + \cdots \tag{26}$$

The smoothing problem becomes one of finding the a_i coefficients which minimize the function corresponding to potential energy shown as

$$A = \iint (\sigma - P)^2 dxdy \tag{27}$$

where P is the smoothing approximate value.

For function A to be minimal

$$\frac{\partial A}{\partial a_i} = 0 \tag{28}$$

This equation defines a set of linear equations. For a smoothing function of a given order, the a_i coefficients are easily obtained.

Assuming the smoothed stress, σ^*, in an element can be interpolated from the smoothed nodal value, $\bar{\sigma}^*$, is

$$\{\sigma^*\} = [N^*]\{\bar{\sigma}^*\} \tag{29}$$

where [N*] is the interpolation function. If the same interpolation function is used with the displacement shape function, the smoothed stress is one order higher than the approximate solution.

In place of P(x,y) using Eq. (29) the function corresponding to potential energy is rewritten

$$A = \int_V \tfrac{1}{2}\left(\{\sigma^h\} - [N^*]\{\bar{\sigma}^*\}\right)^T \left(\{\sigma^h\} - [N^*]\{\bar{\sigma}^*\}\right) dv \tag{30}$$

For function A to be minimal, a set of linear equations are needed by a more accurate nodal value of stress can be calculated;

$$\frac{\partial A}{\partial \bar{\sigma}^*} = \int_V [N^*]^T \left(\{\sigma^h\} - [N^*]\{\bar{\sigma}^*\}\right) dv = 0 \tag{31}$$

From Eq. (31), an explicit formula is derived by which nodal stress can be calculated;

$$[M]\{\bar{\sigma}^*\} = \int_V [N^*]^T \{\sigma^h\} dv \tag{32}$$

or

$$\{\bar{\sigma}^*\} = [M]^{-1} \int_V [N^*]^T \{\sigma^h\} dv \tag{33}$$

where

$$[M] = \int_V [N^*]^T [N^*] dv \tag{34}$$

Matrix [M] has the structure of a classical mass matrix. In some studies, matrix [M] is used as a lumped form to avoid the difficulty of inverting a consistent matrix and simple iteration can be used to obtain the solution to Eq. (32) or (33).

We used the consistent form of matrix [M] in the local smoothing procedure for a bilinear four-node element with 2×2 gauss rule shown in **Fig.3**.

Taking sampling points at the four points of the 2*2 gauss rule, a discrete expression for one bilinear isoparametric element is obtained from Eq.(32);

$$[S]\begin{Bmatrix} \bar{\sigma}_1^* \\ \vdots \\ \bar{\sigma}_4^* \end{Bmatrix} = \{F\} \tag{35}$$

where

$$[S] = \begin{bmatrix} \sum_{i=I,IV} N_1^*(\xi_i,\eta_i) N_1^*(\xi_i,\eta_i) & \cdots & \sum_{i=I,IV} N_1^*(\xi_i,\eta_i) N_4^*(\xi_i,\eta_i) \\ \vdots & \ddots & \vdots \\ \sum_{i=I,IV} N_4^*(\xi_i,\eta_i) N_1^*(\xi_i,\eta_i) & \cdots & \sum_{i=I,IV} N_4^*(\xi_i,\eta_i) N_4^*(\xi_i,\eta_i) \end{bmatrix} \tag{36}$$

$$\{F\} = \begin{Bmatrix} \sum_{i=I,IV} N_1^*(\xi_i,\eta_i)\sigma_i \\ \vdots \\ \sum_{i=I,IV} N_4^*(\xi_i,\eta_i)\sigma_i \end{Bmatrix} = \begin{Bmatrix} \sigma_I \\ \sigma_{II} \\ \sigma_{III} \\ \sigma_{IV} \end{Bmatrix} \tag{37}$$

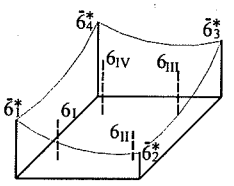

Fig.3 Local smoothing by extrapolation

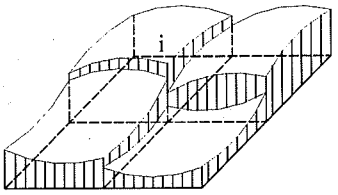

(a) without nodal averaging

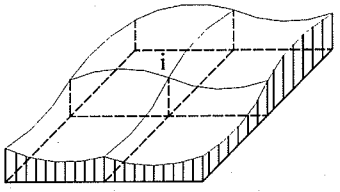

(b) nodal averaging

Fig.4 Nodal averages

Local smoothing is extrapolation of the nodal value $\overline{\sigma}^{*}_{I-4}$ from the values on the gauss points, σ_{I-IV}. It does not produce unique values for the stresses at nodal points; therefore, arithmetic averages of nodal values must be calculated. The smoothed variables of different elements at the same node should be averaged as shown in **Fig.4**.

The local smoothed procedure for strain is the same as the procedure for stress introduced above. It is easily inserted in the programming code because evaluations of the appropriate ε^{*} and ε^{h} quantities are possible using a part of the existing codes within the FEM scheme.

(3) Example of an error estimate

The effectiveness of this error estimate method is shown in the following as example. In **Fig.5** a saturated sand block 4m long and 2m high is compressed at the top surface by a uniformly distributed load. The load increases linearly to 100kN/m until t=10 seconds. The right and left sides are freely in displaced and undrained. The top surface is freely displaced and drained. The bottom is fixed and has an undrained boundary. The parameters used for simulation are same as the Edosaki sand 1 given in **Table 2**.

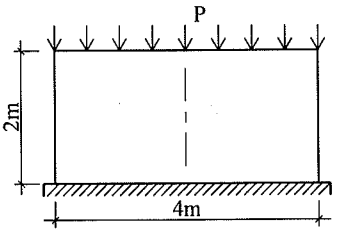

Fig.5 Example of error estimate

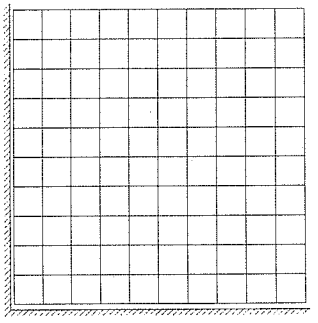

Fig.6 100-element mesh

The right half part was analyzed because of the symmetry of the model and 16-, 100-, and 400-element meshes are used in the error estimation. The 100-element mesh is shown in **Fig.6**.

In the case of 100 elements, the relative errors of strain at times t=2, 4, and 6s are shown in **Fig.7**. The maximum value of the relative percentage error, η_{max}, that occurring at the right top corner is given. Clearly, the error of strain increases with the increases in the strain and load.

Fig.8 shows the contour of relative error for three meshes of different element size and number: 16, 100, and 400 elements. A comparision of the relative errors of strain at point A with coordinates (1.6,1.6) at time t=2s for the 16, 100, and 400 element cases shows clearly that a reduction in element size reduces error.

Point A can be taken as a sample point for the global distribution error because it was selected randomly. **Fig.9** shows the relationship between the error in point A and the number of elements in a doubled notched specimen to demonstrate the effectiveness of the application of our error estimate method to the elasto-plastic analysis of saturated soil. The sloping line is in good agreement with other findings[22]. Although no analytical result is given for comparison, the tendency for convergence with this method is reliable.

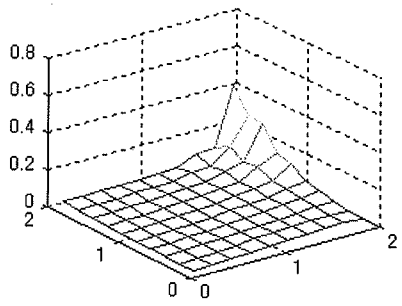

t=2s, η_{max}=40.19%

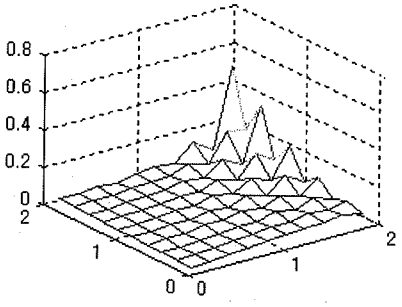

t=4s, η_{max}=48.79%

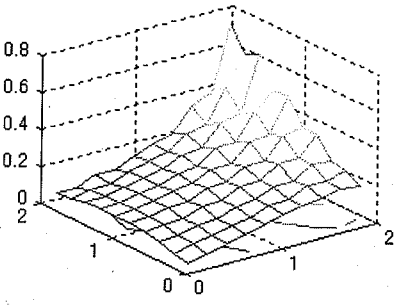

t=6s, η_{max}=71.34%

Fig.7 Relative errors at different times for the case of 100 elements

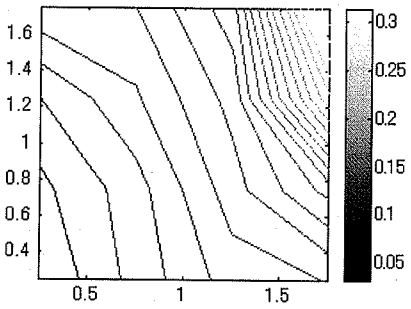

16 elements, η_A=27.13%

Fig.8(1) Relative error contours for different meshes at t=2s

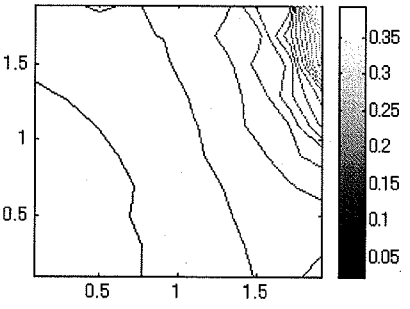

100 elements, η_A=11.25%

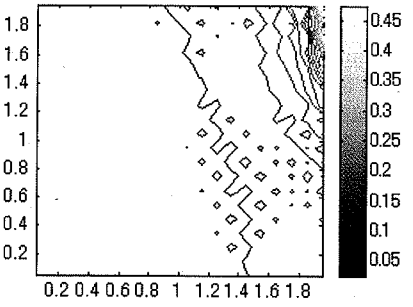

400 elements, η_A=6.25%

Fig.8(2) Relative error contoursfor different meshes at t=2s

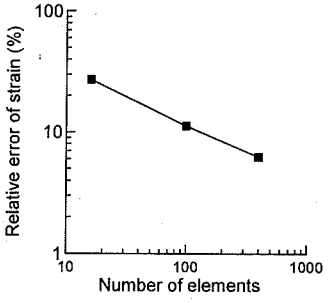

Fig.9 Double notched specimen

4. MESH REFINEMENT

The error for every element is obtained from the error estimate process. The next step is mesh refinement, implemented for elements for which the errors exceed an acceptable limit, in order to improve the accuracy of the finite element approximation. If improvement of accuracy is taken as the target of the adaptivity procedure and the error estimation gives a correct indication, then mesh refinement is the only way to the target. Mesh regeneration based on error estimation also is an effective adaptive procedure, but

in consideration of economy, in this paper in which non-linear dynamic analysis was used, the mesh refinement method was selected.

There are four kinds of mesh refinement methods:

(1) *h*-refinement; reduce the size, *h*, of the elements in high error regions;

(2) *p*-refinement: increase the order, *p*, of the polynomail shape function in high error regions;

(3) *hp*-refinement: simultaneous application of both the *h*- and *p*-refinements;

(4) *r*-refinement: relocate the nodes.

A *h*-adaptive technique[20] was used in which the adaptive process is executed by element error measures in order to allocate elements for generating a mesh with the smallest number of elements and, at the same time, to obtain the required accuracy. The *h*-adaptive technique involves two methods: mesh regeneration and simple mesh refinement, a fission scheme. Mesh regeneration is a means to regenerate a new mesh in the global mesh as indicated by the mesh density obtained in the error estimation process. Data transfer is needed also to move the elements and nodal variables from the old mesh to the new mesh. The fission scheme refines the mesh by fissioning those elements with large error into smaller, equal-sized elements then transferring the variables of the nodes and elements from the old mesh to the new mesh by an interpolation procedure. A comparison of these two schemes, clearly shows that the latter involves less computation than the former. Data transfer in the latter scheme is local whereas in the former it is global. Taking into account the thousands of time increment steps in the dynamic analysis, the fission scheme saves computation and improves accuracy.

In the refinement process, an acceptable relative error limit $\overline{\eta}$ must first be given. If the relative error, η_i, of the *i*th element exceeds this limit, then the element is fissioned into four elements. This process is illustrated in **Fig.10**. The initial mesh is shown as mesh-a. After error estimation, the relative error for element 5 exceeds the error limit, and the element is fissioned into four elements: 5, 7, 8, and 9. Five new nodes, 13, 14, 15, 16, and 17, are created in the mid of four sides and the center of the element. The new mesh refined at the first step is shown as mesh-b. The parameters of element 5 in mesh-a are transferred to elements 5, 7, 8 and 9 in mesh-b, and the variables of the new elements are interpolated from the variables of element 2 in mesh-a. The pore pressure values of the new child elements are same as the pore pressure value of the old parent element. The displacement, velocities, and accelerations of the new nodes also are

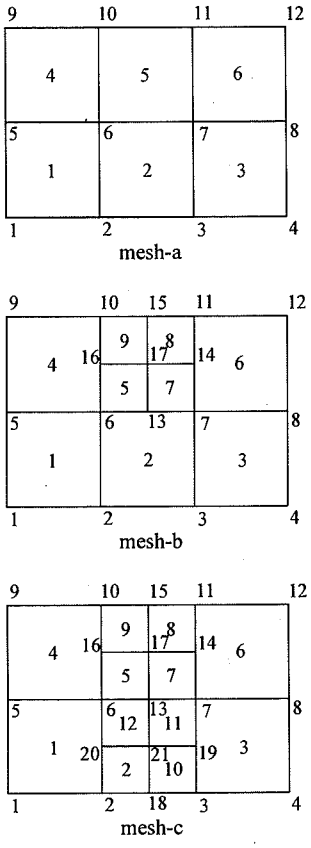

Fig.10 Fission process

interpolated from the values of the old nodes in mesh-a. The next calculation step is based on mesh-b. In that step, element 2 exceeds the limit of error, and new elements and new nodes are created. The difference is that a node is created in the mid of side 7-6, a new node need not be created on this side. The refined mesh is shown as mesh-c.

When an element is fissioned next to an unfissioned one, slave nodes are created, e. g., node 13 in mesh-b **Fig.10**. The motion of slave node 13 should be governed by the constraint of compatibility,

$$\{V_{13}\} = [T]\begin{Bmatrix} V_6 \\ V_7 \end{Bmatrix} \tag{18}$$

where [T] is a linear operator which enforces compatibility and $\{V_6\}$ and $\{V_7\}$ are the velocities of the master nodes. When node 13 is midway between nodes 6 and 7, [T] is defined by [**I**/2,**I**/2], in which **I** is a unit matrix. The equation of motion is not evaluated at the slave node. Instead the nodal forces at the slave nodes are added to the forces at the corresponding master nodes;

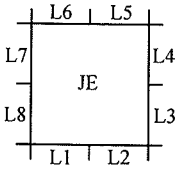

Fig.11 NABOR array

Table 1 NABOR array for the element 2

mesh	JE	L1	L2	L3	L4	L5	L6	L7	L8
b	2	0	0	3	3	7	5	1	1
c	2	0	0	10	10	12	12	1	1

$$\begin{Bmatrix} F_6 \\ F_7 \end{Bmatrix} = \begin{Bmatrix} F_6 \\ F_7 \end{Bmatrix}^* + [T]^T \{F_{13}\} \qquad (19)$$

where $\{F_{13}\}$ are the nodal forces at the slave node and $\{F\}^*$ those at the nodes 6 and 7 prior to the consideration of $\{F_{13}\}$, This is the standard technique for treating constraints in explicit methods.

To clarify the interrelationship between the old and new nodes and elements, requires an elaborate data structure in the process of node and element creation.

To develop master and slave nodes during the fission process an important array NABOR(NE,8), composed of the eight neighboring element numbers of a concerned element are used (**Fig.11**).

NE is the number of the element. To clarify the use of the array, consider mesh-b in **Fig.10** with element 5 already fissioned into element 5, 7, 8, and 9. Also consider mesh-c obtained by fissioning the element 2 to element 2, 10, 11 and 12. The NABOR array for element 2 is given in **Table 1** for both meshes. The first thing to note is that the zero entries for L1 and L2, indicate a boundary at the bottom of element 2. Therefore, a new node needs to be created (node 18) which is a master node. Next, L3=L4=3 indicates that element 3 extends along the entire side of element 2. Therefore a new node (node 19) must be created, which is a slave node. Now, L5=7 and L6=5, therefore a node already exists (node 13) which is a slave node in mesh-b, and, it becomes a master node when element 2 is fissioned.

5. NUMERICAL EXAMPLES

(1) Compression of saturated soil

This is an example of the simulated compression of saturated soil taking into account large deformation, in which *h*-adaptive FE analysis is implemented within the period of compression before liquefaction. The soil block is 2m long by 2m high, and analysis

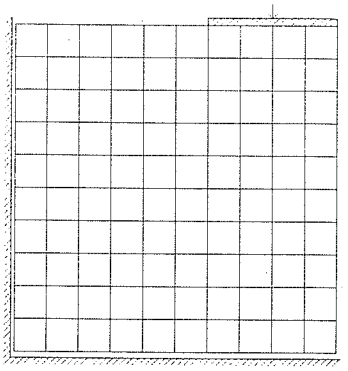

Fig.12 Compression of saturated soil

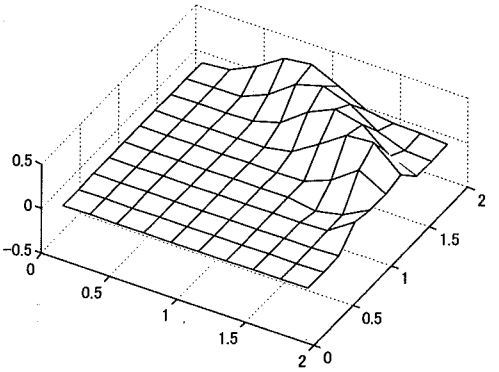

Fig.13 Relative error before refinement

begins with a 100-element mesh, as shown in **Fig.12**. The parameters of soil used for analysis are those of the Edosaki sand 1 defined in **Table 2**. The initial stress of elements are calculated with gravity. Displacement of nodes perpendicular to the boundary side is constrained on the left and bottom. A drained boundary condition is present only on the upper surface. A stepwise load is applied to the right side of the top surface of the block through a rigid plate, 0.8m long, without weight. The load is increased linearly to 20kN/m until t=2 seconds.

The saturated sand which is Enshyunada sand with relative density Dr=40% and initial void ratio e_0=0.992 is described by a cyclic elasto-plastic model. four-node quadralitera isoparametric element is used. Error of shear strain is estimated. The relative error limit $\overline{\eta}$ is 25%. The relative error distribution before mesh refinement is given as **Fig.13**. A large shear strain bound is appeared.

The refined meshes at time t=1sec and t=2sec are given in **Fig.14**, (a) and (b). The elements in the strain bound are refined.

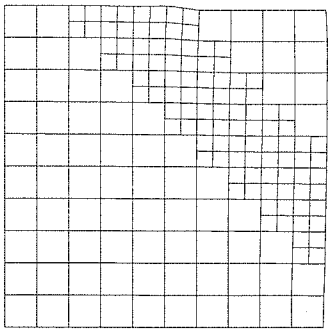

(a) t=1sec, 178 elements

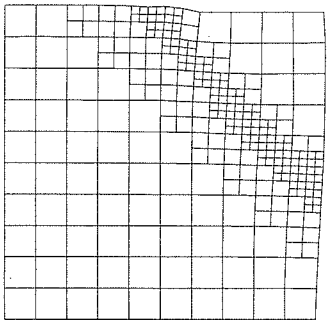

(b) t=2sec, 274 elements

Fig.14 Refined meshes

In this example, *h*-adaptive FE method is implemented in elasto-plastic analysis of saturated soil during the period without liquefaction. When location phenomenon is appeared, the error of shear strain is increasing evidently with increasing of shear strain. Error estimator evaluates errors successfully shown in **Fig.13**. At the same time, fission scheme is used in the area with large error value indicated by error estimate. It's no doubt that our method is applicable to nonlinear analysis without liquefaction.

(2) Simulation of shaking table experiment

The aim of this example is to check the efficiency of *h*-adaptive FE method applied to nonlinear analysis of liquefied soil. Hamada[21] et. al.(1994) did a shaking table experiment of saturated sand in which flow process of liquefied soil was given. The experimental equipment and the process of experiment are shown in **Fig.15**. First, a strong vibration, which the maximum value of accelerate is 100 gal, acts on the shaking test table until time t=7sec. This vibration causes the saturated soil liquefied. Then inclined the soil container to a certain angle (4.2%) in order to let the liquefied sand flow by gravity. The process of inclining begins from horizontal angle at time

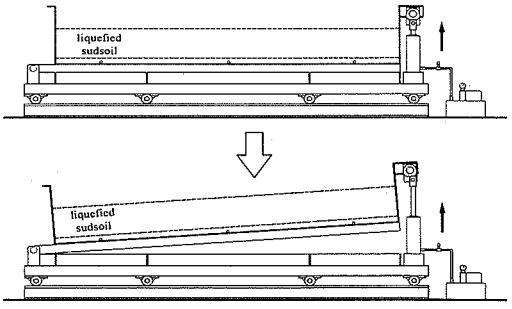

Fig.15 Shaking table test procedure

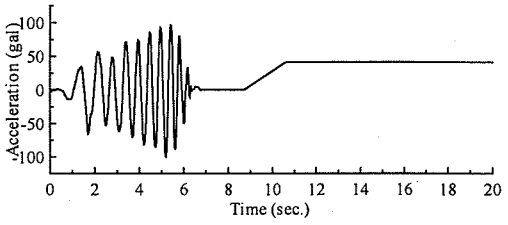

Fig.16 Time history of acceleration input

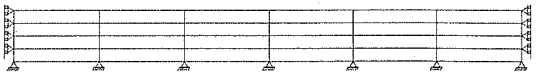

Fig.17 Initial mesh for liquefied sand flow

t=8.7sec and reach to the angle 4.2% at time t=10.6sec. Enshyunada sand with relative density Dr=40% and initial void ratio e_0=0.992 is used in the experiment.

A time history of acceleration shown in **Fig.16** is used to simulate this experimental process.

H-adaptive FE analysis is applied to simulate this experiment. The initial mesh with 24 elements is shown in **Fig.17**. The upper surface is drained boundary. Four-node isoparametric element is adopted. Error of strain is evaluated in error estimation. Because the aim of this example is to check efficiency of adaptive FE method in liquefaction process, the fission scheme starts at time t=8.7sec.

After the strong vibration from t=0sec to t=7.0sec, the saturated soil in the containor is liquefied. When liquefaction happens reduction of effective stress and lose of stiffness and strength of soil. Inclining the container, liquefied soil flows driven by gravity. The flow causes large deformation and high value of discretizition error. Before the liquefaction is onset, the error value is not so large, even though distribution

of error is fluctuate in space. But after the onset of liqufaction the high values of error concentrate in the regions with large deformation. For this reason, adaptive FE method is more effective in the flow analysis of liquefaction. In this example, the adaptive mesh refinement for liquefied soil starts from the time that the flow of liquefied ground starts. The final refined mesh is given in **Fig.18**. The relative error limit $\overline{\eta}$ is 30%. We can find that the elements where large deformation occurs, in other words, where errors are large, are fissioned step by step and the sizes of these elements become small.

The final surfaces of soil calculated for 3 cases were compared in **Fig.19**. In case a and c, 720 elements fixed mesh and 24 elements fixed mesh were used without adaptive mesh refinement. In case b, we used adaptive mesh refinement with 24 elements as the initial mesh. We can find that although the final surface calculated with fixed 24-element mesh is coarse, but the final surface calculated by *h*-adaptive FE method from 24-elements mesh is almost as fine as that calculated with fixed 720-element mesh. The calculation time in case a is about 20 hours, but the calculation time in case b is about 11 hours in the same computer. We can get the conclusion that the level of accuracy of finite element method is raised while the calculation work is reduced by using adaptive mesh refinement. This result can be explained easily by the mechanizm of adaptive technique. In adaptive analysis, the local elements with large error but not global mesh are refined, thus the small-sized elements with fine accuracy are used in the region where fine mesh is needed and number of degree of freedom is used efficiently. That's the reason why the result in case b can reach almost same accuracy as the result in case a.

From this example, we can find that h-adaptive FE method can be applied effectively to liquefaction period of elasto-plastic analysis.

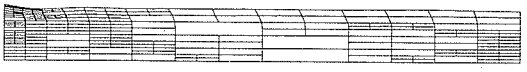

Fig.18 Final mesh (number of elements 366)

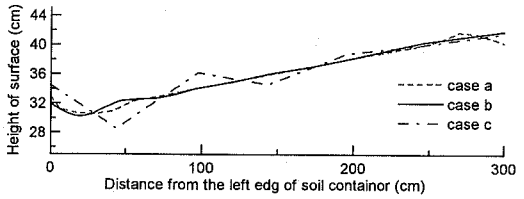

Fig.19 Final soil surface

(3) Earthquake response of embankment

In this example, *h*-adaptive FE method is applied in an earthquake response analysis with updated Langrangian method of embankment sitting on liquefiable soil. An overall elasto-plastic process including liquefaction is given. The efficiency of our method used in practical engineering is checked.

The model of embankment and soil layer is shown in **Fig.20**. The embankment is 2m wide on the top and 20m wide in the bottom. There are two kinds of soil without water in the embankment, Edosaki sand and crushed stone. The soil region we considered is 60m wide and 12m deep. There are two kinds of saturated soil, Edosaki sand and silica in the soil layers. The dynamic parameters of these soils are shown in **Table 2**.

Table 2 Parameters of soil(t,m,s)

Material parameter	Edosaki sand 1	Crushed stone	Edosaki sand 2	silica
Density $\rho(t/m^3)$	1.75	1.54	1.857	1.990
Coefficient of permeability k(m/s)	-	-	1.7E-5	2.5E-5
Initial void ratio e_0	0.856	0.856	0.856	0.676
Compression index λ	0.0264	0.0264	0.0264	0.0250
Swelling index κ	0.0055	0.0055	0.0055	0.0025
Initial shear modulus ratio G_0/σ_{m0}	829	829	829	1280
Over consolidation ratio	1.0	1.0	1.0	1.0
Phase transformation stress ratio M_m	0.91	0.91	0.91	0.91
Failure stress ratio m_f	1.12	1.12	1.12	1.51
Hardening parameter B_0	3000	3000	3000	5000
Hardening parameter B_1	0.0	0.0	0.0	0.0
Hardening parameter C_f	-	-	60	100
Plastic reference stain	-	-	0.01	0.004
Elastic reference strain	-	-	0.03	0.09
Dilatancy parameter D_0	0.0	0.0	5	1.2
Dilatancy parameter n	0.0	0.0	1.2	4.0

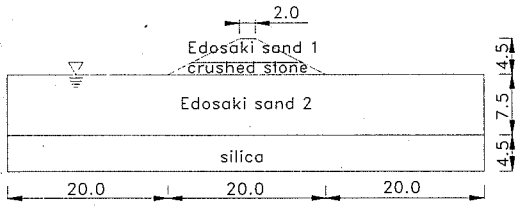

Fig.20 Embankment example

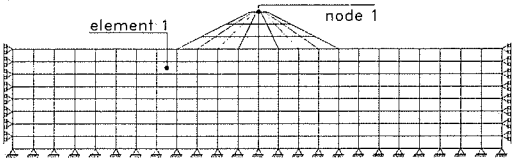

Fig.21 Initial mesh (216 elements)

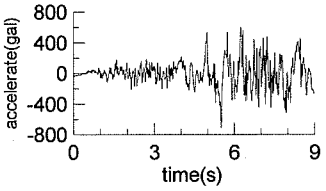

Fig.22 Input acceleration

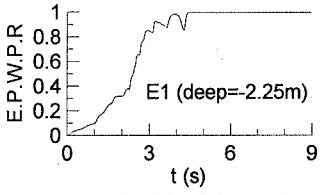

Fig.23 EPWPR of element 1

In **Fig.21**, the initial mesh with 216 elements is shown. The displacement of bottom boundary are fixed, side boundary is fixed in horizontal direction.

We use a time history of horizontal acceleration shown in **Fig.22** as input load. It was recorded in a strong earthquake, the maxmum value is 722 gal. Only 9 seconds is used in our analysis.

The curve of extra pore water pressure ratio of element 1 is given in **Fig.23**. When the value turns to 1.0, the soil is liquefied. We can find that the soil begin to turn into liquefaction state at time t=4.5 sec. We give the analysis results from t=0 second to t=9 second. In this period, the saturated soil shows all states of a liquefaction process, from elastic state to plastic state.

Bilinear isoparametric four-node element is adopted. Considering that different kinds of soil cause

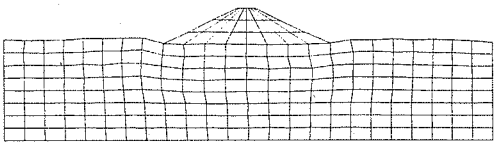

(a) t=7 sec, 216 elements

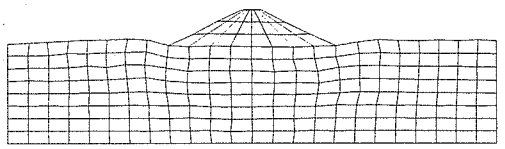

(b) t=8 sec, 216 elements

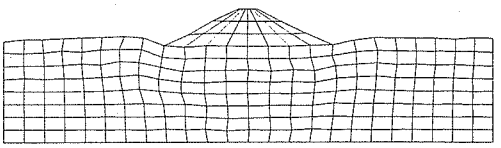

(c) t=9 sec, 216 elements

Fig.24 Mesh for large deformation without adaptivity

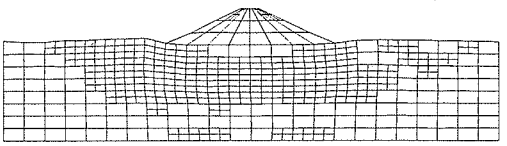

(a) t=7 sec, 435 elements

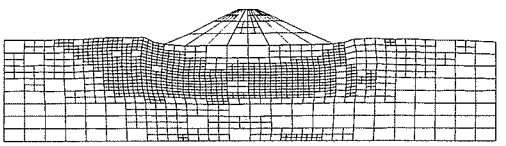

(b) t=8 sec, 906 elements

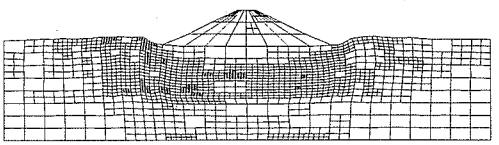

(c) t=9 sec, 1422 elements

Fig.25 Refined mesh for large deformationwith adaptive FEM

the strain discontinue in the joint surface, the L_2-norm of effective stress is selected to evaluate the error. The initial mesh with 216 elements is given in **Fig.21.**

In **Fig.24**, (a), (b) and (c), the meshes at t=7,8,9 second analyzed by fixed 216-element meshes are given respectively. The stress and strain in the region besides the foot of embankment and under the embankment are larger than other region. The value of error in these regions is increased.

In **Fig.25**, (a), (b) and (c) refined meshes analyzed by h-adaptive FEM with updated Lagrangian method are given. The elements in the region with large error, as same as where we mentioned before, are refined step by step. The mesh is turning fine while the number of elements is increasing.

In **Figs.26** and **27**, the horizontal and vertical displacements of node 1 are compared between the adaptive FEM case and FEM case. The elements in the region with large error are refined. The elements in this region are also with large deformation and strain. They are the main part of the whole mesh which affects the displacement of the embankmen. It's evident that refinement of these elements improves the accuracy of the embankment displacement result. From the difference between the two lines is enlarged with mesh being refined, we can find that adaptive FE method improves analysis result efficiently.

As a comparision, we also give the mesh results of FEM and adaptive FEM with small deformation in **Figs.28** and **29** respectively. Although the general deformation due to liquefation are not so large, but there are some region with large deformation, especially in the areas near or under the embankment.

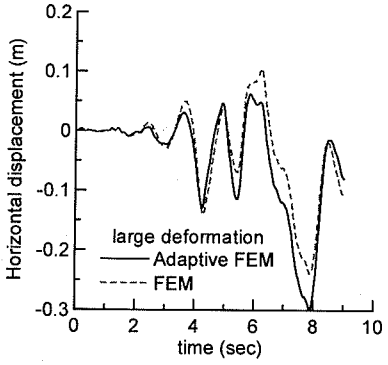

Fig.26 Horizontal displacement of node 1 for large deformation

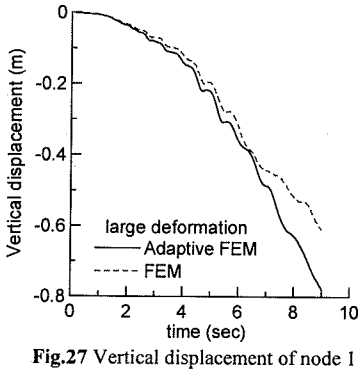

Fig.27 Vertical displacement of node 1 for large deformation

It's easy to find the difference between the two adaptive FEM results, with infinitesimal deformation assumption and with finite deformation theory. The deformation of the last case shown in **Fig.29** are larger than the deformation of the other case shown in **Fig.25**, and the errors of the last case are also larger. For this reason, the elements number of refined mesh of the last case is more than that of the other case.

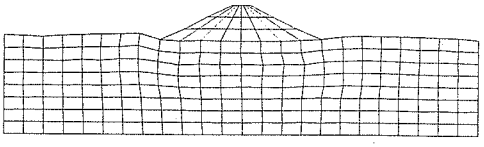

(a) t=7 sec, 216 elements

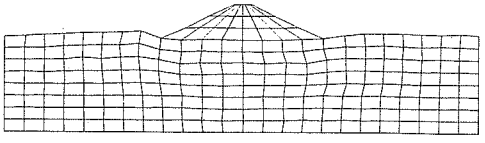

(b) t=8 sec, 216 elements

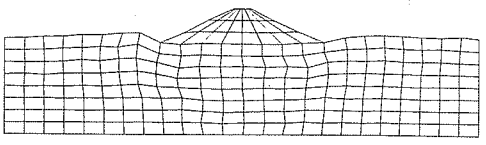

(c) t=9 sec, 216 elements

Fig.28 Mesh for small deformation without adaptivity

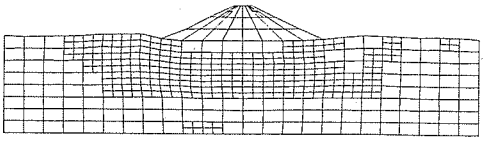

(a) t=7 sec, 432 elements

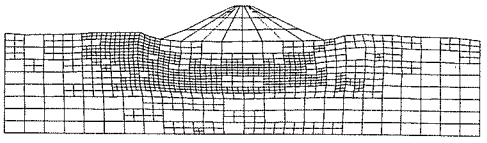

(b) t=8 sec, 945 elements

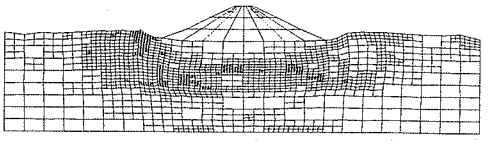

(c) t=9 sec, 1506 elements

Fig.29 Refined mesh for small deformation with the adaptive FEM

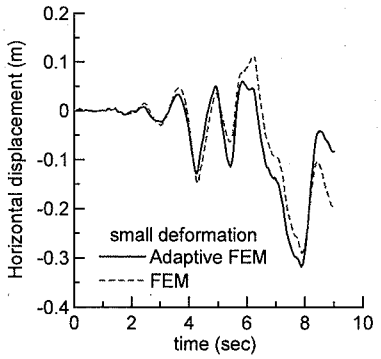

Fig.30 Horizontal displacement of node 1 for small deformation

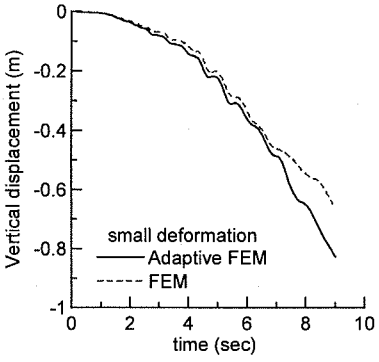

Fig.31 Vertical displacement of node 1 for small deformation

The horizontal and vertical displacements in node 1 in two cases are given in **Figs.30** and **31**. The same phenomenon as **Figs.26** and **27** occurs although the deformed meshes, number of refined elements and the displacements are not same as those in large deformation case. The comparison between **Figs.27** and **31** indicates that the displacements of node 1 with large deformation theory are larger than those with infinitesimal deformation assumption.

By this example, *h*-adaptive FE method is demonstrated to be effective in application to elasto-plastic analysis of saturated soil including an overall liquefaction process. No matter in large deformation case or in small deformation case, this methods works well.

6. CONCLUSIONS

This paper applied adaptive technique to non-linear FE analyses of saturated soil considering large deformation including liquefaction phenomenon. We used fission procedure belong to the *h*-refinement indicated by the error measure of elements. The approximation is successively refined as to satisfy the predetermined standard of accuracy, and the efficiency of this method was confirmed in the finite element analyses. This method is easy to applied to solve practical and engineering problem. In transient analysis, the limits of error are from 2.5%-15%[8)-12)]. There are less papers which introduce adaptive mesh refinement applied in dynamics analysis. Here, in dynamics analysis of adaptive mesh refinement,the limits of error are 20%-30%. The results of our examples are acceptable

A posteriori error estimate based on L_2 norm of strain or stress error was adopted in this paper. It can estimate the error of elements after every step of calculation in nonlinear FE analyses of soil effectively. Smoothing variables procedure includes variables extrapolation from the value in gauss points and nodal values average. In a transient analysis of saturated soil, both strain and stress can be used to estimate errors. But in a dynamic analysis of saturated soil, strain gives more smooth distribution of error than stress. This method is easy to implement into any code and the calculation based on this method is very simple as well as the advantage in saving computation time is evident. This is a reliable indicator for mesh refinement.

The program developed for liquefaction analysis was modified by using this theory. Three numerical examples were given to demonstrate the efficiency of our method. These were compression of saturated sand caused by a stepwise loading, flow of liquefied sand problems considering large deformation which are elasto-plastic analysis without liquefaction and the analysis of liquefied soil problems respectively and a non-linear dynamic analysis problem of saturated soil including liquefaction. The results we have obtained show that this adaptive scheme is capable of achieving substantial improvements in accuracy under a limit computational effort. Generally, an adaptive mesh is capable of achieving one order higher level of accuracy as a fixed mesh with less than half of the computational resource.

ACKNOWLEDGMENT: The author is thankful to Dr. Y. Di for providing the LIQ2D-Large deformation program. Thanks also go to Dr. Y. Moon for providing the simulation results of shaking table experiment with 720 elements mesh.

REFERENCES

1) Oka, F., Yashima, A., Shibata, T., Kato, M. and Uzuoka, R.: FEM-FDM coupled liquefaction analysis of a porous soil using an elasto-plastic model, *Applied Scientific Research*,

Vol. 52, pp. 209-245, 1994.

2) Oka, F., Yashima, A., Tateishi, A., Taguchi, Y. and Yamashita, S.: A cyclic elato-plastic constitutive model for sand considering aplastic-strain dependence of the shear modulus, *Geotechnique*, Vol. 49, No. 5, pp. 661-680, 1999.
3) Oka, F., Yashima, A., Kato, M. and Sekiguchi, K.: A constitutive model for sand based on the non-linear kinematic hardening rule and its application, *Proceedings of 10th World Conference on earthquake Engineering*, Barcelona, pp. 2529-2534, 1992.
4) Biot, MA.: Mechanics of deformation and acoustic propagation in porous media, *Journal of Applied Physics*, Vol. 33, pp. 1482-1498, 1962
5) Akai, K. and Tamura, T.: Study of two-dimensional consolidation accompanied by an elastic plastic constitutive equation, *Proceedings of JSCE*, No. 269, pp. 98-104, 1978.
6) Di, Y. and Sato, T.: Large deformation Dynamic analysis of porou medium using FEM-FDM coupled method, *Advances in Computational Engineering & Sciences (Atluri, S.N.,Nishioka, T. and Kikuchi, M.,Eds.), Chapter 12 Multiphysics & Multibody Dynamic*, Tech Science Press, 2001, (CD-ROM).
7) Di, Y. and Sato, T.: FEM-FDM coupled method for saturated soil analysis considering large deformation, *Proceedings of the 26th JSCE Earthquake Engineering Symposium*, Sapporo, pp. 193-196, 2001.
8) Kelly, D. W., De, J. P., Gago, S. R., Zienkiewicz, O. C. and Babuska, I.: A Posteriori Error Analysis and Adaptive Processes in The Finite Element Method: Part I-Error Analysis, *Int.J.num.Meth.Engng*, Vol. 19, pp. 1593-1619, 1983.
9) Zienkiewicz, O. C., Huang, M.S. and Pastor, M.: Localization Problems in Plasticity Using Finite Elements with Adaptive Remeshing, *Int. J. Nnumer. Aanal. Meth. Geomech.*, Vol. 19, pp.127-148, 1995.
10) Zienkiewicz, O. C. and Zhu, J. Z.: A Simple Error Estimator and Adaptive Procedure for Practical Engineering Analysis, *Int.J.num.Meth.Engng*, Vol. 24, pp. 337-357, 1987.
11) Zienkiewicz, O. C., Liu , Y. C. and Huang, M.S.: Error Estimation and Adaptivity in Flow Formulation for Forming Problems, *Int.J.num.Meth.Engng*, Vol. 25, pp. 23-42, 1988.
12) Zienkiewicz, O. C. and Zhu, J. Z.: Error Estimates and Adaptive Refinement for Plane Bending Problems, *Int.J.num.Meth.Engng*, Vol. 28, pp. 2839-2853, 1989.
13) Mar, A. and Hicks, M.A.: A Benchmark Computational Study of Finite Element Error Estimation, *Int.J.num.Meth.Engng*, Vol. 39, pp. 3969-3983, 1996.
14) Hicks, M.A.: Coupled Computations for an Elastic-Perfectly Plastic Soil Using Adaptive Mesh Refinement, *Int. J. Nnumer. Aanal. Meth. Geomech.*, Vol. 24, pp. 453-476, 2000.
15) Hinton, E. and Campbell, J. S.: Local and global smoothing of discontinuous finite eleemnt functions using a least squares method, *International Journal for Numerical Methods in Engineering*, Vol. 8, pp. 461-480, 1974.
16) Selman, A., Hinton, E. and Bicanic, N.: Adaptive Mesh Refinement for Localised Phenomena, *Computer & Structures*, Vol. 63, pp. 475-495, 1997.
17) Zienkiewicz, O. C., Liu , Y. C. and Huang , M.S.: Error Estimates and Convergence Rates for Various Incompressible Element, *Int.J.num.Meth.Engng*, Vol. 28, pp. 2191-2202, 1989.
18) Kelly, D. W., De, J. P., Gago, S. R., Zienkiewicz, O. C. and Babuska, I.: A Posteriori Error Analysis and Adaptive Processes in The Finite Element Method: Part II-Adaptive Mesh Refinement", *Int.J.num.Meth.Engng*, Vol. 19, pp. 1621-1656, 1983.
19) Belytschko, T. and Tabbara, M.: "H-Adaptive Finite Element Methods for Dynamic Problem, with Emphasis on Localization", *Int.J.num.Meth.Engng*, Vol. 36, 4245-4265, 1993.
20) Belytschko, T., Wong, B. L. and Plaskacz, E. J.: Fission-fussion adaptivity in finite elements for nonlinear dynamics of shells, Computers & Structures, Vol. 33, pp. 1307-1323, 1989.
21) Hamada, M., Sato, H. and Kawakami, T.: A Consideration of the Mechanism for Liquefaction-related Large Ground Displacement, *Aproceedings from the fifth U.S.-Japan workshop on earthquake resistant design of lifeline facilities and countermeasures against soil liquefaction*, Technical Report NCEER-94-0026, pp. 217-232, 1994.
22) Gabaldon, F. and Goicolea, J. M.: Lonear and non-linear finite element error estimation based on assumed strain fields, International Journal for Numerical Methods in Engineering, Vol. 55, pp. 413-429, 2002.

(Received August 22, 2003)